Effects of thermal history on enthalpy relaxation in glasses 7. Thermal time constants

Ian M. Hodge *, Robert Heslin

Rochester Institute of Technology, Rochester, NY 14623, USA

ARTICLE INFO

Article history:
Received 10 August 2004
Received in revised form 13 April 2010
Available online 3 June 2010

Keywords:
<C100>
<E297>
<G200>
<P245>

ABSTRACT

Experimental data on a single polymer sample indicate that the instrumental/sample Green function is essentially a Dirac delta function, with a time constant of 15 s. Distortions of scanned heat capacities over the glass transition temperature range, induced by this Green function, were deconvoluted and the deconvoluted data were found to be independent of heating = cooling rate (apart from temperature shifts), in accordance with expectations. The effects of a single thermal time constant on computed activation energies and different definitions of T_g are discussed. It is suggested that temperature calibration can be compromised by a nonzero thermal time constant.

1. Introduction

The differential scanning calorimeter (DSC) is the instrument of choice for studying the kinetics of enthalpy relaxation within and below the glass transition temperature range. The kinetics are in need of a more precise description, however, because extraction of enthalpy relaxation parameters from DSC data is fraught with technical intricacies that are almost certainly compromised by inadequate consideration of instrumental and sample response characteristics. We present experimental evidence that the Heaviside response function for a DSC polymer sample is well approximated as exponential, resulting in a conveniently simple deconvolution procedure.

The issues of both DSC instrumental response functions and sample temperature gradients have been discussed ever since the technique was first introduced — references are summarized in a 1994 review [1]. O'Neil [2] and Gray [3] were the first to discuss the problem, and further analyses have been given by Mraw [4], Lagasse [5], Sandu and Lund [6], and Van Miltenberg and Cuevas-Diarte [7]. The detailed analyses of Schawe et al. [8–11] are discussed below. Temperature differences across a DSC sample, ΔT_s, have been measured by DeBolt [12] and O'Reilly and Hodge [13], and calculated by DeBolt [12] and Simon [14], but steady state heat diffusion through the thickness of a sample does not account for the data. Thermal diffusivities D_{th} of polymers are typically $1 \pm 0.1 \times 10^{-7}$ m^2 s^{-1}, so that one dimensional heat diffusion through a sample thickness of $d = 0.5$ mm at a cooling or heating rate of 5 K min^{-1} is predicted to produce a temperature difference of about $\Delta T_s \approx Q_h \cdot d^2/2D_{th} \approx (5/60\ \mathrm{K\ s^{-1}})(25 \times 10^{-8}\ \mathrm{m^2})/(2 \times 10^{-7}\ \mathrm{m^2\ s^{-1}}) \approx$ 0.1 K. This is a factor of 6 smaller than the experimental value for a polystyrene sample of thickness 0.5 mm, reported by O'Reilly and Hodge [13]. DeBolt [12] calculated a temperature difference of 0.21 K for a sample of inorganic glass (Vycor) of thickness 0.91 mm. Her calculations included specific boundary conditions and were therefore more rigorous than the crude estimate just given, but it is still of interest to apply to Vycor the present approximate calculation. The thermal diffusivity of Vycor silica glass is 7.5×10^{-7} m^2 s^{-1} [12], so that $\Delta T_s \approx Q_h \cdot d^2/2D_{th} \approx (5/60\ \mathrm{K\ s^{-1}})(83 \times 10^{-8}\ \mathrm{m^2})/(15 \times 10^{-7}\ \mathrm{m^2\ s^{-1}}) \approx$ 0.18 K, comparable with DeBolt's estimate but about a half of the experimental value 0.33 K. Thus the issue is less problematic for inorganic materials, but still significant. The effects of temperature gradients within a sample are not discussed any further here, because our experimental data turned out to be well accommodated by a single time constant with zero temperature gradient.

Several ad hoc techniques for addressing the thermal lag problem have been suggested. Hodge [15,16] attempted to minimize thermal lag effects on relaxation parameters by restricting data analyses to low overshoot heat capacity data (less than 2.0 for the normalized heat capacity), but the present results suggest that this is inadequate. Hutchinson et al. [17,18] assumed a particular computational result to be correct (discussed below), and then processed the experimental data to make them conform to that result. However, no explicit description of their data processing procedure was given. Simon [14] did not consider thermal time constant effects for a poly(ether imide) material.

Schawe et al. [8–11] have given detailed analyses of the problem. They found that linear response theory could be applied to DSC data, which is not obviously so because of feedback loops in the DSC technique. They measured (instrumental + sample) Green functions and computed the true heat capacity of the sample using a deconvolution integral technique. This is undoubtedly the method of choice for rigorous deconvolution of instrumental effects in DSC scans (although Laplace transform techniques might now be easier using commercial

* Corresponding author.
E-mail address: Ian.Hodge@rit.edu (I.M. Hodge).

0022-3093/$ – see front matter © 2010 Elsevier B.V. All rights reserved.
doi:10.1016/j.jnoncrysol.2010.04.037

software such as Matlab®), so that "a fully satisfactory account of thermal lag effects" [1] is probably at hand. The calculation procedure for instrumental effects described here is much simpler, however, and will hopefully encourage a long overdue routine deployment of deconvolution procedures for DSC data before enthalpy relaxation parameters are extracted.

2. Experimental

A single sample of bisphenol A polycarbonate [BPAPC], of mass 21 mg and deliberately irregular in shape to maximize heat transfer effects, was used throughout. Simon [14] has noted that thermal contacts between the sample and the sample pan, and between the sample pan and the instrument cup, are readily minimized. However, no attempt was made to minimize these factors here, in order that a worst case scenario could be analyzed. Scans were performed on a DSC[a1] with liquid nitrogen cooling. A single point temperature calibration was performed using the melting temperature of an indium sample (discussed below). The instrumental/sample response function was determined by programming a change in the heating rate, and recording the evolution of both heating rate and heat flow as the new steady state was reached. The programmed change in scan rate was made above the glass transition temperature range, where the temperature dependence of the sample heat capacity is minimal. Heat flow data were taken directly from the DSC file, and heating rates were computed from the temperature and time data in the same file.

For heat capacity measurements, the sample was equilibrated at 20 K above the upper limit of the glass transition range, cooled at several constant rates to 300 K, held there for 2 min, and reheated at several constant heating rates. No annealing was introduced. Data from the DSC output file were transferred to a text file that was subsequently read and analyzed using Matlab®. Scanned heat capacities were normalized assuming linear temperature dependencies for the glassy and liquid heat capacities.

3. Computational procedures

Heat capacities at constant cooling and heating rates were calculated using the Tool–Narayaswamy–Moynihan (TNM) phenomenology, that has been described in detail elsewhere [1] but is briefly summarized here for convenience. The fictive temperature in the TNM model after n temperature steps of magnitude ΔT_n is given by

$$T_{f,n} = T_0 + \sum_{j=1}^{n} \Delta T_j \left\{ 1 - \exp\left[-\sum_{k=j}^{n} \left(\frac{\Delta T_k}{Q_k \left\{ A \exp\left[\frac{x \cdot h}{T_k} + \frac{(1-x)\cdot h}{T_{f,k}} \right] \right\}} \right)^{\beta} \right] \right\} \tag{1}$$

where A, x and β are adjustable parameters and h, can, in principle, be determined from the change in glassy fictive temperature, T_f, as a function of $Q_c = Q_h$: $h/R = d\ln(Q_c = Q_h)/d(1/T_f)$. The normalized heat capacity is equated to the temperature derivative of $T_{f,n}$. Computation times for each thermal history were typically 2 s using Matlab® on a modest laptop computer running Windows XP. Computational details, most of which differ from earlier accounts, are summarized in Appendix A.

[a1] Thermal analysis TA6900.

4. Computed thermal time constant effects

The effect of an instrumental Green function on calculated heat capacity data was computed using standard linear response formulae for a low pass filter [1]. An instantaneous step increase (Heaviside function) in the sample heat capacity at time t', $\Delta C_p(t')$, produces a time constant delayed (lagged) response given by

$$\Delta C_{p,\mathrm{lag}}\left(t - t'\right) = \Delta C_p(t') \left\{ 1 - \exp\left[\frac{-\left(t - t'\right)}{\tau_{\mathrm{th}}} \right] \right\} \tag{2}$$

where τ_{th} is the thermal time constant. No assumptions or assertions are made about the physical origin of τ_{th}. During heating, the instrumental response to the time-dependent true sample heat capacity is obtained by Boltzmann superposition of the responses described by Eq. (2):

$$C_{p,\mathrm{lag}}(t) = \int_0^t \left(\frac{dC_p}{dt'} \right) \left\{ 1 - \exp\left[\frac{-\left(t - t'\right)}{\tau_{\mathrm{th}}} \right] \right\} dt' \tag{3}$$

For a Dirac delta Green function, deconvolution is readily computed using the expression due to Gray [3]:

$$C_p(t) = C_{p,\mathrm{lag}}(t) + \tau_{\mathrm{th}} \left(\frac{dC_{p,\mathrm{lag}}}{dt} \right) + \text{baseline shift} \tag{4}$$

$$= C_{p,\mathrm{lag}}(t) + \tau_{\mathrm{th}} \cdot Q_h \left(\frac{dC_{p,\mathrm{lag}}}{dT} \right) + \text{baseline shift} \tag{5}$$

The equivalence of Eq. (3) to Eqs. (4) and (5) is proven in Appendix B. The second term on the right hand side of Eq. (5) is henceforth referred to as the Gray correction term. The baseline shift is eliminated when the heat capacity data are normalized, and is ignored here. Integration of Eq. (5), and applying the boundary conditions $C_{p,\mathrm{lag}}(T_{\mathrm{min}}) = C_p(T_{\mathrm{min}}) = C_{pg}(T_{\mathrm{min}})$ and $C_{p,\mathrm{lag}}(T_{\mathrm{max}}) = C_p(T_{\mathrm{max}}) = C_{pl}(T_{\mathrm{max}})$, yields

$$\int_{T_{\mathrm{min}}}^{T_{\mathrm{max}}} C_p dT = \int_{T_{\mathrm{min}}}^{T_{\mathrm{max}}} C_{p,\mathrm{lag}} dT + \tau_{\mathrm{th}} \cdot Q_h \left[C_{p,\mathrm{lag}}(T_{\mathrm{max}}) - C_{p,\mathrm{lag}}(T_{\mathrm{min}}) \right] \tag{6}$$

where C_{pg} and C_{pl} are the glassy and liquid heat capacities, respectively.

In terms of the normalized heat capacities C_p^{N} and $C_{p,\mathrm{lag}}^{\mathrm{N}}$, the expression for the glassy fictive temperature T_f [1] is then, since $C_{p,\mathrm{lag}}^{\mathrm{N}}(T_{\mathrm{max}}) - C_{p,\mathrm{lag}}^{\mathrm{N}}(T_{\mathrm{min}}) = 1.0$,

$$T_f' = T_{\mathrm{max}} - \int_{T_{\mathrm{min}}}^{T_{\mathrm{max}}} C_p^{\mathrm{N}}\left(T'\right) dT' \tag{7}$$

$$= T_{\mathrm{max}} - \int_{T_{\mathrm{min}}}^{T_{\mathrm{max}}} C_{p,\mathrm{lag}}^{\mathrm{N}}\left(T'\right) dT' - \tau_{\mathrm{th}} \cdot Q_h \tag{8}$$

Eq. (8) expresses the fact that the glassy fictive temperature obtained from integration of the lagged normalized heat capacity lies $\tau_{\mathrm{th}} Q_h$ above that obtained from integration of the actual normalized heat capacity. This is the long known effect of heating rate on temperature calibration and, as is also well known, implies that τ_{th} can be determined from temperature calibration as a function of heating rate. However, the present experimental results indicate that this is not true if temperature calibration is performed using a melting standard (such as indium) that is not incorporated into the sample.

Optimizations indicated that the best fit TNM parameters x and h were significantly affected by a nonzero τ_{th}, but that the KWW

parameter β was not. Given the unexpected success of the simple deconvolution procedure described here, however, these results are not reported here.

5. Order of heat capacity deconvolution and normalization

It needs to be established if deconvolution of a normalized heat capacity gives the same result as normalization of deconvoluted data. There is a small difference that is much smaller than typical experimental uncertainty. It is straightforward (see Appendix C) to show that these two protocols produce Gray correction terms that differ by the factor $\left[1 + \tau_{th} \cdot Q_h (d \ln \Delta C_{p,lag}/dT)\right]^{-1}$, where $\Delta C_{p,lag}$ denotes the difference between the observed (lagged) liquid and glassy heat capacities. This factor is computed to be 1.007 using input values of $\tau_{th} = 15$ s (as experimentally determined here), $Q_h = 10$ K min^{-1}, $\Delta C_{p,lag}(T) = C/T$ (the strongest temperature dependence usually observed), and $T = 375$ K. This maximum error of 0.7% can reasonably be neglected compared with the typical experimental scatter of $\pm 2\%$. For the present analyses, data were first normalized and then deconvoluted.

6. Results and discussion

6.1. Experimental Green function and deconvoluted heat capacities

The observed transients in the heating rate and heat flow are shown in Fig. 1. The two curves have almost the same shape but are displaced by about 15 s. The maxima differ by 9%, and the time shifts at elapsed times of 1760 s, 1780 s and 1800 s are 12 s, 15 s and 21 s respectively. The time displacement at half the maximum heights is 14.5 ± 0.5 s, which was rounded off to 15 s and equated to a single thermal time constant. Changes in these time shifts were less than 0.5 K when the two response functions were normalized to the same maximum value. Thus the Green function is close to a Dirac delta function with a time constant of 15 s, and the deconvolution procedure described above is applicable. The experimental heat capacities for which the cooling rate (Q_c) and the heating rate (Q_h) had the same magnitude, are shown in Fig. 2. Fig. 3 shows the deconvoluted scans using a time constant of 15 s. The numerically induced noise in the deconvoluted functions could easily be removed using a moving average, but the non-filtered results are shown here to indicate the raw data. As expected, the original scans exhibit pronounced distortions that increase as $Q_c = Q_h$ increases – in the extreme case of $Q_c = Q_h = 25$ K min^{-1} the overshoot is completely suppressed, for example. For other DSC instruments that accommodate faster controlled cooling/heating rates, this effect could be even greater (if τ_{th} does not decrease correspondingly). On the other hand, the deconvoluted scans all have the same shape and are simply displaced in temperature – the normalized overshoots are consistently 1.5 ± 0.1 for example. This constancy is predicted by the TNM formalism for $Q_c = Q_h$ [19], and since this formalism is known to give an excellent account of DSC scans with no annealing, the accuracy of a Dirac delta Green function is confirmed. This constancy was also used by Hutchinson et al. in their pioneering incorporation of lag effects [17,18]. The effects of sample weight and morphology on this result will be the subjects of future studies.

Normalized heat capacity maxima $C^N_{p,max}$ for the deconvoluted data are plotted in Fig. 4 as a function of $Q_c = Q_h$, for five values of τ_{th}: 5, 10, 12, 15, and 20 s. Uncertainty bars for $C^N_{p,max}$ are omitted for clarity, but are typically ± 0.1. For $\tau_{th} = 15$ s, the deconvoluted overshoots were 1.49 ± 0.02 except for the maximum $Q_c = Q_h = 25$ K min^{-1} datum, which was 1.53. This time constant is the same as that inferred from the Q_h transient results.

6.2. Calculated effects of a single thermal time constant

Representative computed normalized heat capacities for $Q_c = Q_h = 10$ K min^{-1} are shown in Fig. 5. The unlagged normalized heat capacity C^N_p computed from the temperature derivative of Eq. (1) is indicated by the solid line. The lagged heat capacity $C^N_{p,lag}$, computed from Eq. (3) with $\tau_{th} = 15$ s, is indicated by the dotted line. The maximum in $C^N_{p,lag}$ lies exactly on the high temperature side of the maximum in C^N_p, consistent with Eq. (5) when $dC_{p,lag}/dT = dC_p/dT = 0$. The dashed line in Fig. 5 is for $C^N_{p,lag}$ that has been corrected for the lag induced temperature shift $\Delta T = \tau_{th} \cdot Q_h$ appearing in Eq. (8). The effect of a thermal time constant is seen to be significant, in agreement with

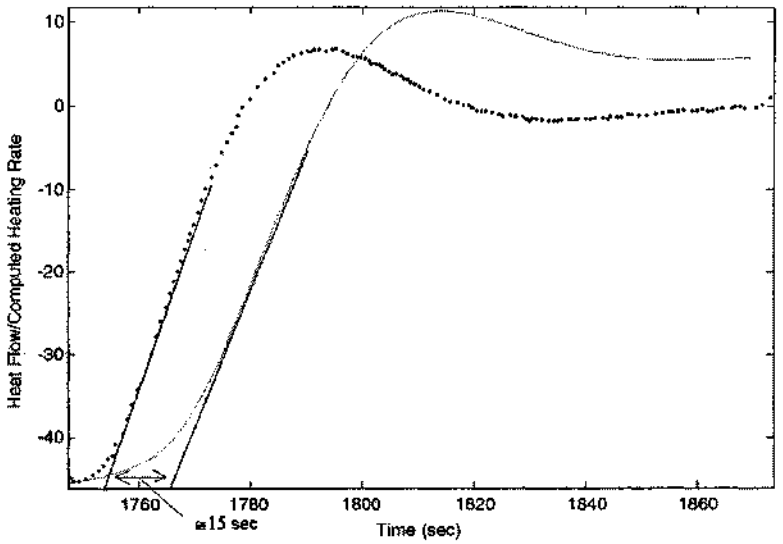

Fig. 1. Experimental transients in computed heating rate (dotted curve) and heat flow (solid line) following a programmed change in heating rate from 20 K/min to 40 K/min. The scales of the y axis are arbitrary and chosen only for convenience.

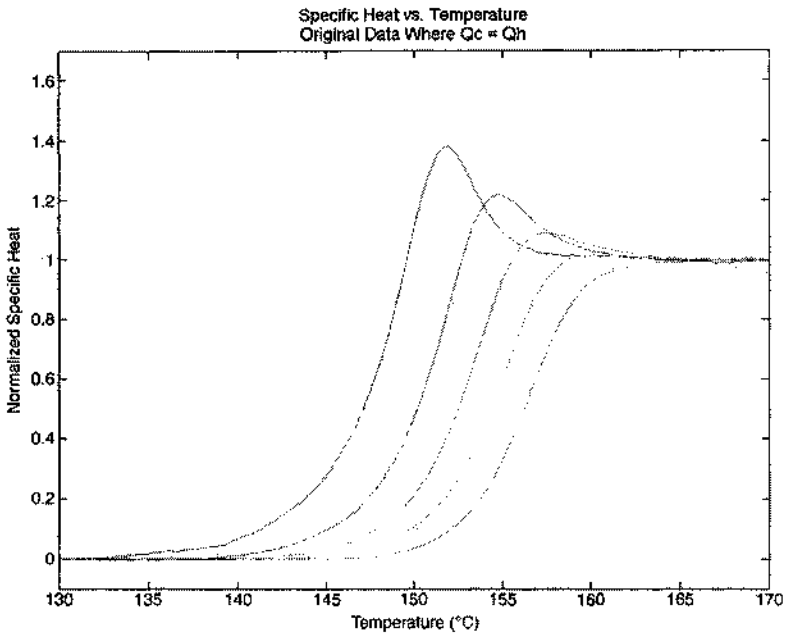

Fig. 2. Normalized experimental heat capacities for different $Q_c = Q_h$ rates (from left to right: 5, 10, 15, 20 and 25 K min^{-1}).

the experimental data shown in Fig. 2, even at the normal heating rate of 10 K min^{-1} — the computed maximum normalized heat capacity at that heating rate decreases from 1.73 to 1.31, for example. Thus Hodge's suggestion that lag effects can be neglected for $C_p^N < 2$ [15,16] is probably too optimistic, although the thermal time constant for the carefully prepared samples in those studies was undoubtedly less than 15 s.

6.3. Calculated effects on "T_g" and apparent activation energies

Calculated values of $C_{p,max}^N$, T_f and $T_{g,mid}$, computed with a single set of TNM parameters for a series of scans in which $Q_c = Q_h$ were varied from 2.5 K min^{-1} to 40 K min^{-1}, for three values of τ_{th} (0, 5, 10 s), are summarized in Table 1. The values of τ_{th} are deliberately smaller than the 15 s determined here, in anticipation of typical τ_{th} values being less

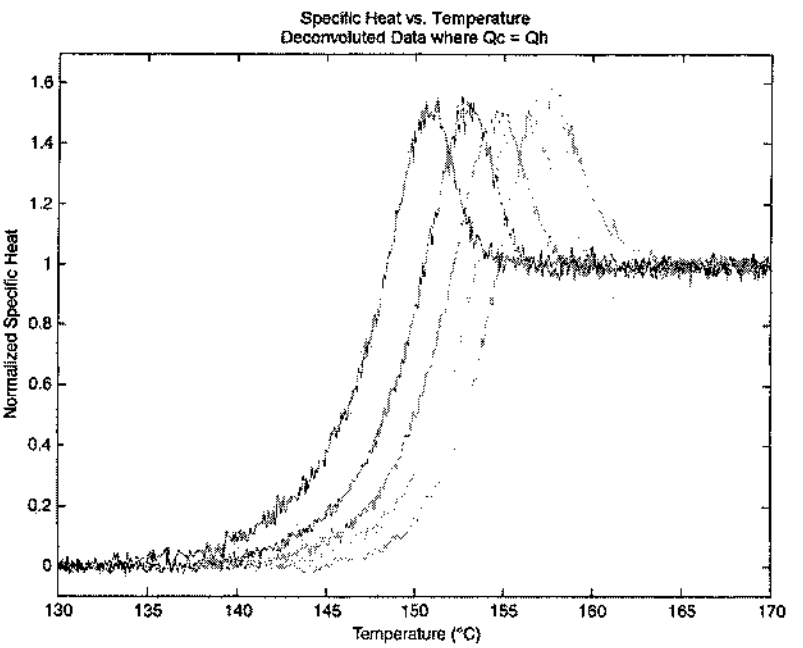

Fig. 3. The same data as those shown in Fig. 2, after deconvolution using the value $\tau_{th} = 15$ s.

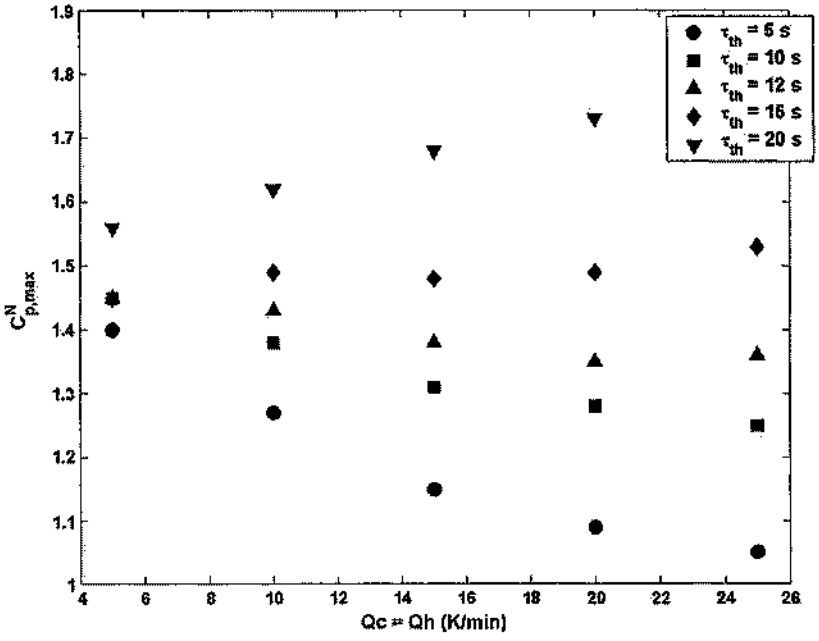

Fig. 4. Normalized heat capacity maxima for the deconvoluted experimental data, as a function of $Q_c = Q_h$ and τ_{th}.

than the worst case value measured here. The ratio $R \equiv C^N_{p,max}(\tau_{th}>0)/C_{p,max}N(\tau_{th}=0)$ computed from the data in Table 1 is a linear function of $Q_h \cdot \tau_{th}$: $R = 1.0 - 0.082 \cdot Q_h \cdot \tau_{th}$ (not shown). No effort was made to derive this result. Plots of ln $(Q_c = Q_h)$ vs. $1/T_{g,mid}$ are shown in Fig. 6. Corresponding data for thermal histories in which the heating rate was kept constant at 10 K min^{-1}, and only the cooling rate varied, are summarized in Table 2. Plots of ln (Q_c) vs. $1/T_{g,mid}$ are shown in Fig. 7.

The effects of thermal lag on effective activation energies determined from the cooling rate dependencies of T_f and $T_{g,mid}$ are informative. For the $Q_c = Q_h$ data, excellent Arrhenius fits are found for the T_f data for all values of τ_{th}, with an activation energy of $h/R = 81.2$ kK that agrees with the input value of 80.5 kK within estimated numerical uncertainties. This is as it should be, since T_f is established before lag-affected heating occurs (confirmed by integrations of C_p^N that yielded the same values for T_f for all values of τ_{th}). Very different results were obtained from analyses of $T_{g,mid}$, however.

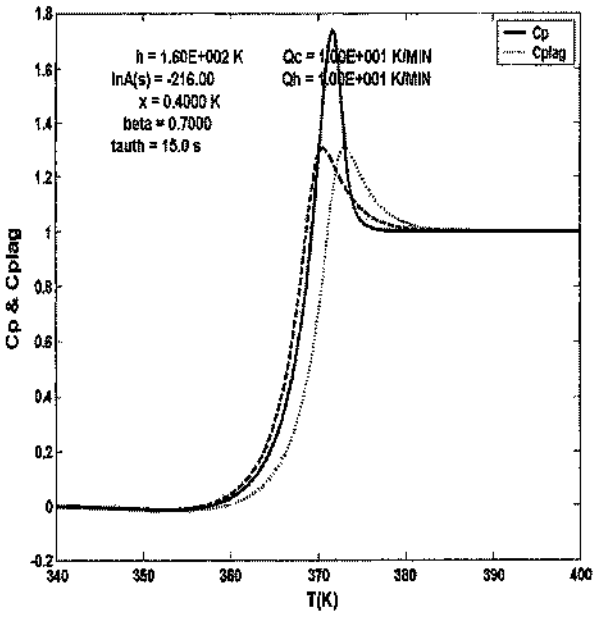

Fig. 5. Computed normalized heat capacities. Solid line: unlagged values; dotted line: lagged values for $\tau_{th} = 15$ s, without any temperature correction $Q_h\tau_{th}$; dashed line: lagged values for $\tau_{th} = 15$ s, with temperature correction $Q_h\tau_{th}$.

Table 1
Calculated effects of thermal time constants, computed values of T_f and $T_{g,mid}$ as a function of $Q_c = Q_h$ and τ_{th}. Input: $\Delta h^*/R = 80.52$ kK, ln A(s) = −216.00, $x = 0.400$, and $\beta = 0.650$. No annealing.

$Q_c = Q_h$	τ_{th} (s)	$C^N_{p,max}$	T_f	$T_{f(corr)}$[a]	$T_{g,mid}$	$T_{g,mid(corr)}$[a]	$Q_h \cdot \tau_{th}$ (K)	R (see text)
40	0	1.581		366.71	369.39	369.39	0	1
	5	1.156	369.95	366.62	371.62	368.29	3.33	0.73
	10	1.000	373.26	366.59	373.03	366.36	6.67	(0.63)
20	0	1.581	365.57	365.57	368.23	368.23	0	1
	5	1.367	367.13	365.46	369.49	367.82	1.67	0.86
	10	1.154	368.81	365.48	370.46	367.13	3.33	0.73
10	0	1.581	364.42	364.42	367.08	367.08	0	1
	5	1.493	365.17	364.34	367.73	366.90	0.83	0.94
	10	1.365	366.00	364.33	368.33	366.66	1.67	0.86
5	0	1.581	363.30	363.30	365.93	365.93	0	1
	5	1.551	363.62	363.20	366.23	365.81	0.42	0.98
	10	1.492	364.04	363.21	366.58	365.75	0.83	0.94
2.5	0	1.581	362.18	362.18	364.79	364.79	0	1
	5	1.572	362.30	362.09	364.91	364.70	0.21	0.99
	10	1.551	362.50	362.08	365.09	364.67	0.42	0.98
1.25	0	1.581	361.05	361.05	363.66	363.66	0	1
	5	1.579	361.09	360.99	363.69	363.59	0.10	1
	10	1.572	361.18	360.97	363.78	363.57	0.21	0.99

[a] Corrected for temperature shift $Q_h\tau_{th}$.

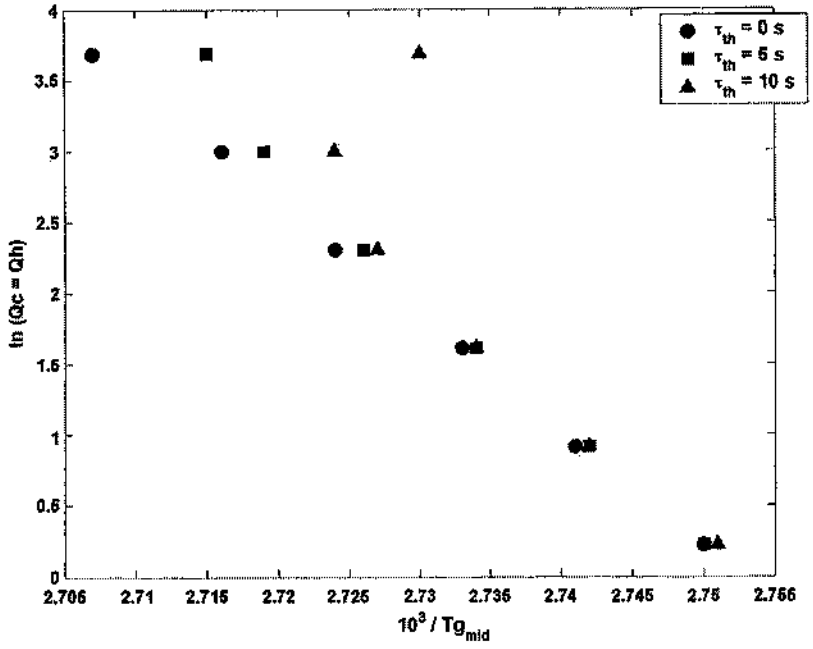

Fig. 6. Arrhenius plot of $\ln[(Q_c = Q_h)/(K/min)]$ vs $10^3 / [1 / T_{g,mid}(K)]$.

Although h/R is the same as that for T_f' for $Q_c = Q_h$ and $\tau_{th} = 0$, consistent with an invariant curve shape for non-lagged data at constant Q_c/Q_h, h/R varies with $Q_c = Q_h$ for $\tau_{th} > 0$ and for the highest values of $Q_c = Q_h$ it becomes unphysically negative. Since $\tau_{th} > 0$ for all DSC experiments, values of $T_{g,mid}$ obtained from unconvoluted data are clearly an unacceptable metric for a "glass transition temperature".

Unacceptable results were also found for the constant $Q_h = 10\ K\ min^{-1}$ data (Fig. 7). Although the Arrhenius plots for each value of τ_{th} are linear with the same slopes (within ±1%), the apparent activation energy is 350×10^3 K, a factor of 4.3 larger than the TNM input value of 80.5×10^3 K. The results shown in Fig. 7, if they were observed experimentally, would look seductively consistent with one another with a constant activation energy, which is not equal to the input h/R however and is clearly incorrect. These results illustrate why it is inappropriate to determine effective activation energies from the cooling rate dependence of $T_{g,mid}$ at fixed Q_h.

Table 2
Computed values of T_f and $T_{g,mid}$ (K) as a function of Q_c and τ_{th} for $Q_h = 10\ K\ min^{-1}$. Input: $h^*/R = 80.52$ kK, ln A(s) = −216.00, $x = 0.400$, and $\beta = 0.650$. No annealing.

Q_c K min^{-1}	τ_{th} (s)	$C_{p,max}^N$	T_f(K)	$T_{f(corr)}$ (K)	$T_{g,mid}$ (K)	$T_{g,mid(corr)}$ (K)
80	0	1.243	367.84	367.84	367.84	367.84
	5	1.212	368.59	367.76	368.50	367.67
	10	1.140	369.41	367.74	369.13	367.46
40	0	1.311	366.69	366.69	367.61	367.61
	5	1.268	367.43	366.60	368.26	367.43
	10	1.185	368.26	366.59	368.87	367.20
20	0	1.419	365.56	365.56	367.34	367.34
	5	1.356	366.30	365.47	367.99	367.16
	10	1.286	367.13	365.46	368.60	366.93
10	0	1.581	364.42	364.42	367.08	367.08
	5	1.493	365.17	364.34	367.73	366.90
	10	1.365	366.00	364.33	368.33	366.66
5	0	1.825	363.28	363.28	366.88	366.88
	5	1.699	364.02	363.19	367.53	366.70
	10	1.530	364.85	363.18	368.14	366.47

(a) Corrected for temperature shift $Q_h \tau_{th}$.

6.4. Temperature calibration

The temperature shift of $Q_h \cdot \tau_{th}$ exhibited in Eq. (8) can, as noted, be used in principle to determine τ_{th} from the heating rate dependence of the onset melting temperature of a standard material, typically indium for polymer investigations. We present evidence that indicates that this approach is flawed, and that temperature calibration using pure indium (or any other metallic calibrant) is almost certainly inaccurate.

Temperature calibration of the present DSC using pure indium indicated a consistent time constant of 5 ± 0.5 s, compared with 15 ± 2 s obtained from deconvolution analyses for the polymer sample. This discrepancy is attributed mainly to slower heat transfer within the polymer sample compared with metallic indium, although poorer contact between the instrument cup and sample pan for the polymer cannot be excluded as a contributing factor. A better calibration procedure would be to embed the indium calibrant between disks of polymer whose combined thickness equaled the sample under investigation. If the indium melting occurs outside the temperature range of interest for the polymer sample, temperature calibration could then be accomplished at the same time as heat capacity acquisition. Such experiments are planned.

Acknowledgement

It is a pleasure to thank A. Langner for assistance with operating the TA6900 DSC.

Appendix A. Updated computational procedures

(1) Computations are made using Matlab® (previously Fortran). (2) Temperature steps are 0.1 K for both rate cooling and rate heating stages, compared with 1.0 K and 0.2 K used earlier.(3) The stretched

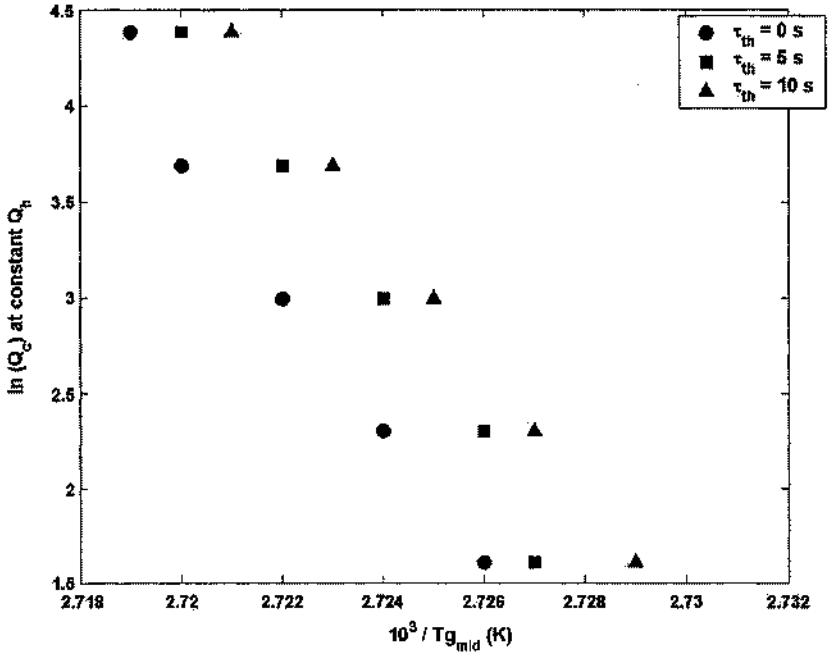

Fig. 7. Arrhenius plot of ln[(Q_c)/(K/min)] at constant Q_h vs 10^3 / [1 / $T_{g,mid}$(K)].

exponential function is used explicitly, rather than being expressed as a Prony series of exponentials.(4) The temperature steps for computing heat capacities in excess of 1.0 during heating are, as before, reduced in inverse proportion to the heat capacity calculated in the previous step [6,16]:

$$\Delta T_k = \frac{\Delta T}{C^N_{p,k-1}} \tag{A1}$$

where $\Delta T = 0.1$ K is the fixed temperature step interval used for the cooling cycle and when $C_p^N \leq 1.0$ during heating. This adjustment is more accurate than before because of the smaller $\Delta\tau$ used, and ensures that changes in fictive temperature during each step are small enough to lie within the linear relaxation regime $\Delta T_f < 1$ K [6,16].Although neither annealing nor relaxation parameter extraction is part of the present results, the modified procedures for implementing them are given here for the sake of completion.(5) The annealing time is divided into 100 intervals per decade (compared with five intervals per decade used earlier).(6) Subdivision of the annealing time is implemented with the *logspace* function in Matlab®. This function creates logarithmic evenly spaced intervals between user-specified limits, chosen to be 0.1 seconds and the annealing time. This increases the number of time intervals at very short times compared with earlier procedures, and thus yields a more accurate computation of annealing for glasses with elevated initial fictive temperatures (that can relax very quickly).(7) Calculated data at the irregularly spaced temperature intervals generated by Eq. (A1) are cubic spline interpolated, instead of linearly interpolated, to generate C_p^N at uniformly spaced temperatures (needed for comparison with experimental data).(8) Extraction of enthalpy relaxation parameters from experimental data is performed using the Matlab® optimization function *fminsearch*, that employs the Nelder–Mead simplex method. This is an improvement over the Fortran Marquardt algorithm used earlier, because it allows all four relaxation parameters to be obtained, compared with only three parameters for Marquardt. Typical optimization times are 30–35 min.

Appendix B. Consistency of Eqs. (3) and (5)

Differentiation of Eq. (3) yields

$$\frac{dC_{p,\mathrm{lag}}}{dt} = \frac{d}{dt}\int_0^t \left(\frac{dC_p}{dt'}\right)\left\{1-\exp\left[\frac{-\left(t-t'\right)}{\tau_{\mathrm{th}}}\right]\right\}dt' \tag{B1}$$

$$= \int_0^t \frac{\partial}{\partial t}\left(\frac{dC_p}{dt'}\right)\left\{1-\exp\left[\frac{-\left(t-t'\right)}{\tau_{\mathrm{th}}}\right]\right\}dt' \tag{B2}$$

$$= \int_0^t \left(\frac{dC_p}{dt'}\right)\left\{\frac{1}{\tau_{\mathrm{th}}}\exp\left[\frac{-\left(t-t'\right)}{\tau_{\mathrm{th}}}\right]\right\}dt' \tag{B3}$$

Subtracting and adding $1/\tau_{\mathrm{th}}$ from the integrand in Eq. (B3) gives

$$\frac{dC_{p,\mathrm{lag}}}{dt} = \int_0^t \left(\frac{dC_p}{dt'}\right)\left\{\frac{1}{\tau_{\mathrm{th}}}\exp\left[\frac{-\left(t-t'\right)}{\tau_{\mathrm{th}}}\right]-\frac{1}{\tau_{\mathrm{th}}}+\frac{1}{\tau_{\mathrm{th}}}\right\}dt' \tag{B4}$$

$$= \int_0^t \left(\frac{dC_p}{dt'}\right)\left\{\frac{1}{\tau_{\mathrm{th}}}\exp\left[\frac{-\left(t-t'\right)}{\tau_{\mathrm{th}}}\right]-\frac{1}{\tau_{\mathrm{th}}}\right\}dt' + \int_0^t \frac{1}{\tau_{\mathrm{th}}}\left(\frac{dC_p}{dt'}\right)dt' \tag{B5}$$

$$= -\frac{1}{\tau_{\mathrm{th}}}C_{p,\mathrm{lag}} + \int_0^t \frac{1}{\tau_{\mathrm{th}}}\left(\frac{dC_p}{dt'}\right)dt' \tag{B6}$$

$$= \frac{1}{\tau_{\mathrm{th}}}\left(C_p - C_{p,\mathrm{lag}}\right) \tag{B7}$$

Multiplying through by τ_{th} yields Eq. (5).

Appendix C. Order of normalization and deconvolution

Deconvolution of normalized data, $C^{N}_{p,lag}$, yields

$$C^{N}_{p} = C^{N}_{p,lag} + \tau_{th}\left(\frac{dC^{N}_{p,lag}}{dt}\right) \tag{C1}$$

This is to be compared with the expression obtained by normalizing previously deconvoluted experimental data $C_{p,lag}$, derived as follows. First, we note that Eq. (4) also applies to C_{pg} and ΔC_p:

$$C_{pg} = C_{pg,lag} + \tau_{th}\left(\frac{dC_{pg,lag}}{dt}\right) \tag{C2}$$

and

$$\Delta C_{p} = \Delta C_{p,lag} + \tau_{th}\left(\frac{d\Delta C_{p,lag}}{dt}\right) \tag{C3}$$

where the baseline shift has been set to zero because it cancels out after normalization. Second, $C^{N}_{p,lag}$ and $C_{p,lag}$ are related by

$$C_{p,lag} = C_{pg,lag} + C^{N}_{p,lag}\cdot\Delta C_{p,lag} \tag{C4}$$

the time derivative of which is

$$\frac{dC_{p,lag}}{dt} = \frac{dC_{pg,lag}}{dt} + \frac{dC^{N}_{p,lag}}{dt}\cdot\Delta C_{p,lag} + C^{N}_{p,lag}\cdot\frac{d\Delta C_{p,lag}}{dt} \tag{C5}$$

Substitution of Eqs. (C4) and (C5) into Eq. (4) gives

$$C_{p} = C_{pg,lag} + C^{N}_{p,lag}\cdot\Delta C_{p,lag} + \tau_{th}\left(\frac{dC_{pg,lag}}{dt} + \frac{dC^{N}_{p,lag}}{dt}\cdot\Delta C_{p,lag} + C^{N}_{p,lag}\cdot\frac{d\Delta C_{p,lag}}{dt}\right) \tag{C6}$$

The normalized unlagged heat capacity is

$$C^{N}_{p} = \frac{C_{p}-C_{pg}}{\Delta}C_{p} \tag{C7}$$

Insertion of Eqs. (C6), (C2) and (C3) into Eq. (C7) yields

$$C^{N}_{p} = \frac{C_{pg,lag} + C^{N}_{p,lag}\cdot\Delta C_{p,lag} + \tau_{th}\left(\frac{dC_{pg,lag}}{dt} + \frac{dC^{N}_{p,lag}}{dt}\cdot\Delta C_{p,lag} + C^{N}_{p,lag}\cdot\frac{d\Delta C_{p,lag}}{dt}\right) - C_{pg,lag} - \tau_{th}\left(\frac{dC_{pg,lag}}{dt}\right)}{\Delta C_{p,lag} + \tau_{th}\frac{d\Delta C_{p,lag}}{dt}} \tag{C8}$$

$$= \frac{C^{N}_{p,lag}\cdot\Delta C_{p,lag} + \tau_{th}\left(\frac{dC^{N}_{p,lag}}{dt}\cdot\Delta C_{p,lag} + C^{N}_{p,lag}\cdot\frac{d\Delta C_{p,lag}}{dt}\right)}{\Delta C_{p,lag} + \tau_{th}\frac{d\Delta C_{p,lag}}{dt}} \tag{C9}$$

$$= \frac{C^{N}_{p,lag}\left(\Delta C_{p,lag} + \tau_{th}\frac{d\Delta C_{p,lag}}{dt}\right) + \tau_{th}\left(\frac{dC^{N}_{p,lag}}{dt}\cdot\Delta C_{p,lag}\right)}{\Delta C_{p,lag} + \tau_{th}\frac{d\Delta C_{p,lag}}{dt}} \tag{C10}$$

$$= C^{N}_{p,lag} + \frac{\tau_{th}\left(\frac{dC^{N}_{p,lag}}{dt}\cdot\Delta C_{p,lag}\right)}{\Delta C_{p,lag} + \tau_{th}\frac{d\Delta C_{p,lag}}{dt}} = C^{N}_{p,lag} + \frac{\tau_{th}\left(\frac{dC^{N}_{p,lag}}{dt}\right)}{1 + \tau_{th}\left(\frac{1}{\Delta}C_{p,lag}\right)\frac{d\Delta C_{p,lag}}{dt}} \tag{C11}$$

$$= C^{N}_{p,lag} + \frac{\tau_{th}\left(\frac{dC^{N}_{p,lag}}{dt}\right)}{1 + \tau_{th}\frac{d\ln(\Delta C_{p,lag})}{dt}} \tag{C12}$$

Comparison of Eqs. (C1) and (C12) reveals that the Gray correction terms for the two protocols differ by the factor $=[1+\tau_{th}d\ln(\Delta C_{p,lag})/dt]^{-1}$, as stated in the text.

References

[1] I.M. Hodge, J. Non-Crystalline Solids 169 (1994) 211.
[2] M.J. O'Neil, Analyt. Chem. 36 (1964) 1238.
[3] A.P. Gray, in: R.S. Porter, F.F. Johnson (Eds.), Analytical Calorimetry, Plenum, New York, 1968, p. 209.
[4] S.C. Mraw, Rev. Sci. Instrum. 53 (1982) 228.
[5] R.R. Lagasse, J. Poly. Sci. Polym. Phys. Ed. 20 (1982) 279.
[6] C. Sandu, D. Lund, Thermochim. Acta 88 (1985) 453.
[7] J.C. Van Miltenburg, M.A. Cuevas-Diarte, Thermochim. Acta 156 (1989) 291.
[8] G.W.H. Hohne, J.E.K. Schawe, Thermochim. Acta 229 (1993) 27.
[9] J.E.K. Schawe, C. Schick, G.W.H. Hohne, Thermochim. Acta 229 (1993) 37.
[10] J.E.K. Schawe, Thermochim. Acta 229 (1993) 69.
[11] J.E.K. Schawe, G.W.H. Hohne, C. Schick, Thermochim. Acta 244 (1994) 33.
[12] M. A. DeBolt, PhD Thesis, Catholic University of America (1976).
[13] J.M. O'Reilly, I.M. Hodge, J. Non-Cryst. Solids 130–133 (1991) 451.
[14] S.L. Simon, Macromolecules 30 (1997) 4056.
[15] I.M. Hodge, Macromolecules 16 (1983) 898.
[16] I.M. Hodge, G.S. Huvard, Macromolecules 16 (1983) 371.
[17] J.M. Hutchinson, M. Ruddy, M.R. Wilson, Polymer 29 (1988) 152.
[18] J.M. Hutchinson, M. Ruddy, J. Polym. Sci. 26 (1988) 2341.
[19] C.T. Moynihan, A.J. Easteal, M.A. DeBolt, J. Tucker, J. Amer. Ceram. Soc. 59 (1976) 12.